

# Optical characterization of Si-doped $\text{InAs}_{1-x}\text{Sb}_x$ grown on GaAs and GaAs-coated Si by molecular-beam epitaxy

W. Dobbelaere, J. De Boeck, P. Van Mieghem, R. Mertens, and G. Borghs  
*Interuniversity Micro-Electronics Center vzw, Kapeldreef 75, B-3001 Leuven, Belgium*

(Received 6 September 1990; accepted for publication 12 November 1990)

Epitaxial layers of Si-doped  $\text{InAs}_{1-x}\text{Sb}_x$  have been grown by molecular-beam epitaxy on GaAs and GaAs-coated Si substrates. The absorption coefficient was measured in the 3–12  $\mu\text{m}$  wavelength range and the experimental data was fit using an analytical expression that was derived from the Kane band model. The fitted value of the Fermi level was used to calculate the electron concentration and the results were compared with doping levels obtained from secondary ion mass spectroscopy and Hall measurements.

## I. INTRODUCTION

$\text{InAs}_{1-x}\text{Sb}_x$  ( $x \approx 0.65$ ) is the III-V compound semiconductor with the smallest band gap, making it a very interesting material for the fabrication of infrared detectors.<sup>1,2</sup> It is essential to have accurate information about the doping properties of this material in order to optimize the device performance. While GaAs is commonly  $n$ -doped with Si,  $\text{InAsSb}$  is usually  $n$ -doped with Se by effusion of  $\text{PbSe}$ . The use of Si as an alternative to Se for the  $n$ -doping of  $\text{InSb}$  has already been investigated<sup>3</sup> and recently the first results of Si-doped  $\text{InAsSb}$  were demonstrated.<sup>4</sup>

In this paper we present a study of the  $n$ -type doping of  $\text{InAs}_{1-x}\text{Sb}_x$  using Si as a dopant. The  $\text{InAs}_{1-x}\text{Sb}_x$  layers were grown on GaAs and Si substrates. These substrates are interesting for the monolithic integration of electronic devices with infrared  $\text{InAs}_{1-x}\text{Sb}_x$  detectors.<sup>5-9</sup> The infrared absorption spectra of the epilayers could be measured accurately over a large wavelength range (3–12  $\mu\text{m}$ ) because the substrates are transparent large band-gap materials. The Si-doped epilayers exhibited a significant shift of the optical gap due to the large bandfilling in the conduction band. This effect was first demonstrated by Burstein<sup>10</sup> and Moss<sup>11</sup> for  $\text{InSb}$ . Following a description of the experimental conditions in Sec. II, we worked out an analytical expression for the absorption coefficient using the Kane band model<sup>12-14</sup> in Sec. III. In Sec. IV we used this theoretical function to fit our experimental results. From these fits, we obtained an accurate value of the Fermi level which was employed in Sec. V to calculate the electron concentration in the epilayers. The calculated carrier concentration was compared with the results of Hall measurements and secondary ion mass spectroscopy (SIMS). In addition we compare the Si-doped  $\text{InAs}_{1-x}\text{Sb}_x$  samples with GaAs reference samples doped under similar circumstances.

At high doping levels, the bandstructure may be disturbed by band-gap narrowing and tailing effects which may be particularly important in the narrow band-gap material that is under consideration in this study. Therefore we estimate the importance of these effects in Sec. VI.

## II. EXPERIMENT

Three 3.3- $\mu\text{m}$ -thick  $\text{InAs}_{1-x}\text{Sb}_x$  epilayers with different doping levels were grown under identical growth condi-

tions. The growths were carried out simultaneously on a piece of GaAs wafer and a piece of GaAs-coated Si. The structure and the growth conditions of the GaAs-coated Si substrate are as described elsewhere.<sup>7</sup> The wafers were degassed for 15 min at 580 °C under As pressure. Then the substrate temperature was lowered to 380 °C and the Sb shutter was opened. The  $\text{As}_2$  and  $\text{Sb}_4$  beam equivalent pressures (BEP) were  $2.5 \times 10^{-7}$  Torr and  $2 \times 10^{-6}$  Torr, respectively. The growth was started at low growth rate (0.5  $\mu\text{m}/\text{h}$ ) and after about 100 nm the In temperature was increased slowly to reach the standard growth rate of 1  $\mu\text{m}/\text{h}$ . The In BEP was  $7 \times 10^{-7}$  Torr. The only difference between the samples was the Si-doping level: (undoped,  $T_{\text{Si}} = 990$  °C,  $T_{\text{Si}} = 1070$  °C). The composition of the epilayers was measured using wavelength dispersive spectroscopy (WDS) and is given in Table I. The accuracy is about 1%. The layer thickness was determined from scanning electron microscopy (SEM) images of cross sections and is also given in Table I.

The infrared transmission of the epilayers was measured with a Pye-Unicam double beam infrared spectrophotometer. Figure 1 shows the room temperature transmission curves for growths A, B, and C on GaAs (a) and on Si (b) substrates. The measurements were not corrected for the spectral response of the GaAs or the Si substrate. A large shift of the transmission edge with Si doping is observed. This can be explained by the large bandfilling that occurs in  $\text{InAs}_{1-x}\text{Sb}_x$  due to the low density of states in the conduction band. The results for the GaAs and the Si substrates are identical except for some differences in the Fabry Perot oscillations below the band gap due to the intermediate GaAs buffer layer on the Si substrate. This agrees with previously published IR measurements of  $\text{InAs}_{1-x}\text{Sb}_x$  epilayers grown on GaAs and on Si substrates.<sup>7</sup> Also, there are some absorption dips from the Si substrate at 77 and 137 meV and the GaAs substrate at 56 and 65 meV. The doped samples also show a significant free electron absorption at small photon energies. The onset of the free electron absorption lies around 0.05 eV for sample B and around 0.1 eV for sample C.

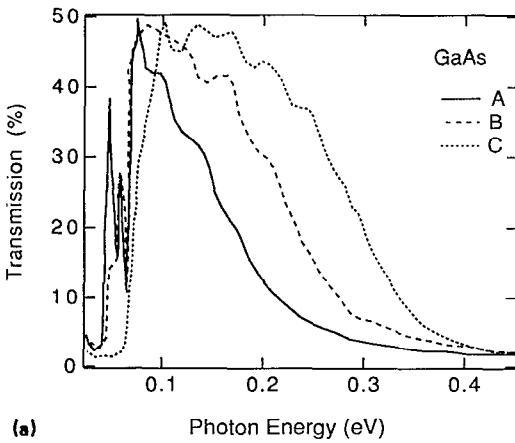
## III. THEORY

In this section we will calculate the interband absorption coefficient and the electron concentration for  $n$ -type

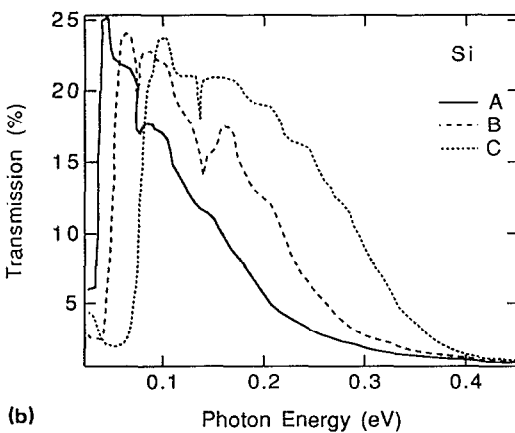
TABLE I. Composition from WDS, Si dopant cell temperature ( $T_s$ ), layer thickness from SEM and room-temperature band gap of  $\text{InAs}_{1-x}\text{Sb}_x$  epilayers grown on GaAs.

Sample	A	B	C
Sb-content (%)	70	68	71
$T_s$ (°C)	...	990	1070
Thickness ( $\mu\text{m}$ )	3.37	3.30	3.27
Band gap (meV)	102.0	101.0	102.7

$\text{InAs}_{1-x}\text{Sb}_x$ . The band structure of a narrow-gap semiconductor such as InSb has been calculated in detail by Kane.<sup>12-14</sup> In this paper we apply Kane's theory to calculate the optical absorption in  $\text{InAs}_{1-x}\text{Sb}_x$  which is the III-V compound semiconductor with the smallest energy band gap (100 meV at 300 K for  $x = 0.65$ ). It is interesting to obtain an approximate analytical expression for the absorption coefficient to fit experimental results. Therefore we will make a few approximations. Since the split off energy  $\Delta$  ( $\approx 0.8$  eV)



(a)



(b)

FIG. 1. Room-temperature transmission spectra of  $\text{InAs}_{0.3}\text{Sb}_{0.7}$  epilayers grown on GaAs (a) and Si (b) with different Si doping levels: A: undoped, B:  $T_s = 990^\circ\text{C}$ , and C:  $1070^\circ\text{C}$ .

is large compared with the band gap  $E_g$  ( $\approx 0.1$  eV), the two-band approximation gives a sufficiently good description of the conduction-band dispersion curve. In that case the conduction-band dispersion curve  $E_c(k)$  is given by Eq. (1). The top of the valence band was taken as the reference energy level.

$$E_c(k) = \frac{\hbar^2 k^2}{2m_0} + \frac{(E_g + \sqrt{E_g^2 + 8P^2 k^2/3})}{2}, \quad (1)$$

where  $P$  is a matrix element between the valence- and conduction-band states and is defined in Ref. 12. It is determined by the atomic properties of the material and is comparable for most III-V compound semiconductors.  $P$  is usually given in terms of an energy  $E_p = 2m_0 P^2 / \hbar^2$  which is equal to 21.11 eV for InAs and 22.49 eV for InSb. Linear interpolation gives a value of  $E_p = 22.1$  eV for  $\text{InAs}_{0.3}\text{Sb}_{0.7}$ .<sup>15</sup> The light hole density of states is much smaller than the heavy-hole density of states so that we will neglect its contribution to the absorption coefficient. Moreover, for the highly degenerate samples that are considered in this paper, the difference in the heavy and light hole dispersion curves makes the light hole absorption contribution take off at significantly higher energies than the heavy-hole contribution. While the conduction-band dispersion curve is calculated directly from the interaction between the conduction band and the valence bands, the heavy-hole dispersion curve is strongly influenced by interactions with higher lying bands.<sup>12</sup> The heavy-hole band is approximately parabolic with an experimentally determined effective mass  $m_{hh} = 0.4m_0$  and is given by

$$E_{hh}(k) = -\frac{\hbar^2 k^2}{2m_{hh}}. \quad (2)$$

The absorption coefficient  $\alpha$  can be calculated as a function of the photon energy  $E$  with Eq. (3).<sup>12,16</sup> This expression is given in SI units, requiring an additional factor of  $1/4\pi\epsilon_0$  with respect to Eq. (35) in Ref. 12.

$$\alpha(E) = \frac{\pi e^2 \hbar}{m_0^2 c n \epsilon_0 E} M_{c-hh}^2(E) \rho_{c-hh}(E) [f_v(E) - f_c(E)]. \quad (3)$$

In this equation,  $n$  is the index of refraction,  $M_{c-hh}^2(E)$  is the square of the optical matrix element between heavy hole and conduction band, averaged over direction, and is given by<sup>12</sup>

$$M_{c-hh}^2(E) = \frac{m_0^2 P^2}{3\hbar^2} \left( 1 + E_g \sqrt{E_g^2 + \frac{8k^2(E)P^2}{3}} \right). \quad (4)$$

The reduced density of states for the heavy hole and conduction band is given by<sup>12,17</sup>

$$\rho_{c-hh}(E) = k(E)^2 \left[ 2\pi^2 \left( \frac{dE_c}{dk(E)} - \frac{dE_{hh}}{dk(E)} \right) \right]^{-1}, \quad (5)$$

where  $dE_c/dk$  and  $dE_{hh}/dk$  are the derivatives of the conduction and valence band dispersion curves. The Fermi Dirac distribution functions  $f_c$  and  $f_v$  of the conduction band and the valence band, respectively, are given by Eq. (6). These functions describe the population effects that occur in the highly doped samples.<sup>16,18,19</sup>

$$f_c = \left[ 1 + \exp\left(\frac{E_c - E_f}{kT}\right) \right]^{-1},$$

$$f_v = \left[ 1 + \exp\left(\frac{E_v - E_f}{kT}\right) \right]^{-1}. \quad (6)$$

For the degenerate  $n$ -type samples that are considered in this paper, we find that  $(E_v - E_f)/kT \ll -1$  so that we can set  $f_v \approx 1$ . The value of the wave vector  $k$  of electrons that are excited by photons with energy  $E$  can be found by setting

$$E = E_c(k) - E_v(k)$$

$$= \frac{\hbar^2 k^2}{2m_0} + \frac{E_g + \sqrt{E_g^2 + 8P^2 k^2/3}}{2} + \frac{\hbar^2 k^2}{2m_{hh}}. \quad (7)$$

We define  $m_r = 1/(1/m_0 + 1/m_{hh})$  as some sort of reduced mass. This equation can be solved for  $k$  and is for simplicity expressed in terms of  $E_p$  instead of  $P$ . The relation  $k(E)$  is given by

$$k^2(E) = \frac{m_r}{\hbar^2} \frac{4E(E - E_g)}{(2E - E_g) + (2m_r/3m_0)E_p} \left( 1 + \sqrt{1 - \frac{4E(E - E_g)}{[(2E - E_g) + (2m_r/3m_0)E_p]^2}} \right)^{-1}. \quad (8)$$

The expression for the absorption coefficient [Eq. (3)] can be rewritten using Eqs. (4)–(7) as

$$\alpha(E) = K \left( 1 + \frac{E_g}{\sqrt{E_g^2 + 8k^2(E)P^2/3}} \right) \frac{1 - (1 + \exp\{[E - \hbar^2 k^2(E)/2m_{hh} - E_f]/kT\})^{-1} k(E)}{\hbar^2/m_r + (4P^2/3)/\sqrt{E_g^2 + [8k^2(E)P^2/3]}} \frac{k(E)}{E}, \quad (9)$$

where  $k(E)$  is given by Eq. (8) so that a completely analytical expression for the absorption coefficient is obtained. The constant  $K$  is given by

$$K = \frac{P^2 e^2}{6\pi c n \hbar \epsilon_0}. \quad (10)$$

From the conduction band dispersion curve (1) and the Fermi level one can calculate the electron density in the conduction band. The number of electrons is given by the integral of the product of the density of states and the Fermi-Dirac distribution function [Eq. (11)].<sup>17</sup> A factor of 2 was added to account for the spin:

$$n = \int_{E_g}^{\infty} \frac{k(E_c)^2}{\pi^2 [dE_c/dk(E_c)]} \frac{dE_c}{1 + \exp((E_c - E_f)/kT)}. \quad (11)$$

The function  $k(E_c)$  is also given by Eq. (8) where  $E$  is replaced by  $E_c$  and  $m_r$  is replaced by  $m_0$ . In the following sections we will use Eq. (9) to fit the experimental absorption curves and we will calculate the electron concentration with Eq. (11).

#### IV. DATA ANALYSIS

From the transmission data and the layer thickness, the absorption coefficient was computed. An optical resonator model was used to eliminate the effect of Fabry-Perot oscillations from the transmission measurements.<sup>20</sup> The absorption spectra were fit with Eq. (9). The amplitude factor  $K$ , the Fermi level  $E_f$ , and the slope  $kT$  were the only fitting parameters. The band gap  $E_g$  (Table I) was calculated using the data from WDS measurements with Eq. (12) where  $x$  is the composition and  $T$  is the temperature.<sup>21</sup>

$$E_g(x, T) = 0.411 - [3.4 \times 10^{-4} T^2 / (210 + T)] - 0.876x + 0.7x^2 + 3.4 \times 10^{-4} x T (1 - x) \text{ (eV)}. \quad (12)$$

Due to the good compositional uniformity we found a nearly identical band gap of  $102 \pm 1$  meV for all the samples at room temperature. This value is very close to the minimal

band gap of 100 meV for material with an Sb content of 65%. Figure 2 shows the experimental absorption spectra together with the fitted curves for samples A, B, and C (grown on GaAs) at 77 and 300 K. Excellent agreement between the calculations and the measurements was observed. Sample A (area  $\approx 0.5$  cm<sup>2</sup>) was smaller than samples B and C (area  $\approx 1.0$  cm<sup>2</sup>) which resulted in a lower accuracy. In the optical cryostat the measurement saturated above 0.35 eV. This part of the measurement was removed from Fig. 2(a). The fitted values of  $K$ ,  $E_f$ , and  $kT$  are listed in Table II. At 300 K, the slope  $kT$  agrees quite well with the expected value (0.0258 eV) but at 77 K there is a large discrepancy between the measured and expected (0.007 eV) values. This phenomenon has been observed in previous experiments for InSb and is explained by Gobel and Fan as a consequence of a warped valence band.<sup>22</sup> They demonstrate that the valence band of InSb is nonspherical, causing the absorption coefficient to increase gradually. At elevated temperatures, this effect is completely masked by the thermal broadening but at low temperatures it determines the slope of the spectrum. The theoretical value of  $K$  ( $2.63 \times 10^{-59}$  J<sup>2</sup> m<sup>2</sup> for  $n = 4$  and  $P$  as mentioned before) is about 1.5 times smaller than the experimental values for  $K$ . This can be explained by the fact that Coulomb interactions were neglected.<sup>16</sup> However, the most important figure of our calculation is the Fermi level which

TABLE II. Value of  $K$ ,  $E_f$ , and  $kT$ , obtained from fit of absorption coefficient with Eq. (9).

Sample	A	B	C
$K$ -300 K ( $10^{-59}$ J <sup>2</sup> m <sup>2</sup> )	3.8	3.7	3.9
$K$ -77 K ( $10^{-59}$ J <sup>2</sup> m <sup>2</sup> )	3.6	3.6	3.8
$E_f$ -300 K (eV)	0.153	0.246	0.323
$E_f$ -77 K (eV)	0.177	0.279	0.362
$kT$ -300 K (eV)	0.026	0.030	0.028
$kT$ -77 K (eV)	0.022	0.019	0.017

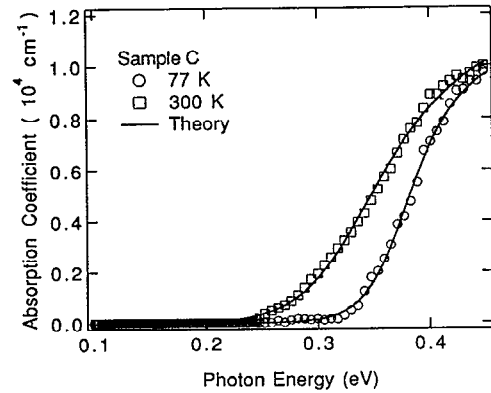
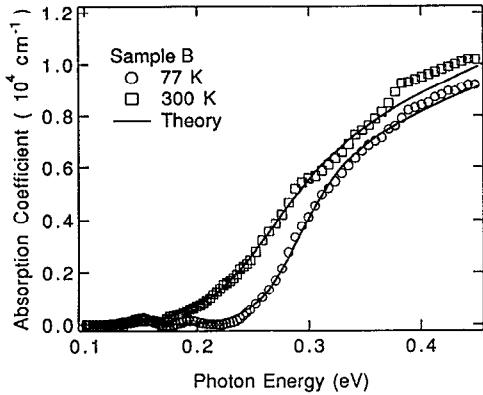
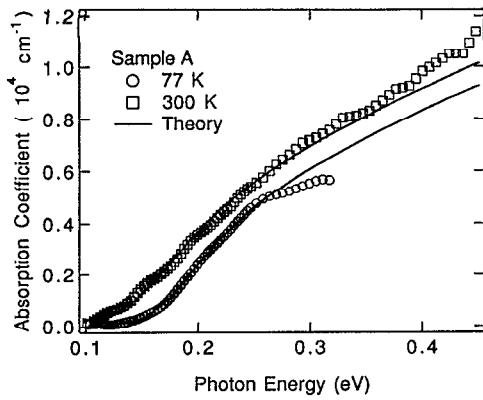


FIG. 2. Absorption spectra (markers) at 300 and 77 K for growths A, B, and C. Solid lines are fit with Eq. (9). The fitting parameters are the scaling factor  $K$ , the Fermi level  $E_f$ , and the slope  $kT$ . The results of the fit are given in Table I.

is relatively insensitive to the approximations made. The temperature dependence of the fitted Fermi levels is shown in Fig. 3. The solid lines are given by  $E_g(T) + [E_f(300) - E_g(300)]$  in order to compare the temperature dependence of the bandgap and the Fermi level. The good agreement indicates that the temperature dependence of the Fermi level can be completely attributed to the variation of the band gap with temperature. This also means that the electron density remains approximately the same between 77 and 300 K. For the undoped sample, the Fermi level is quite

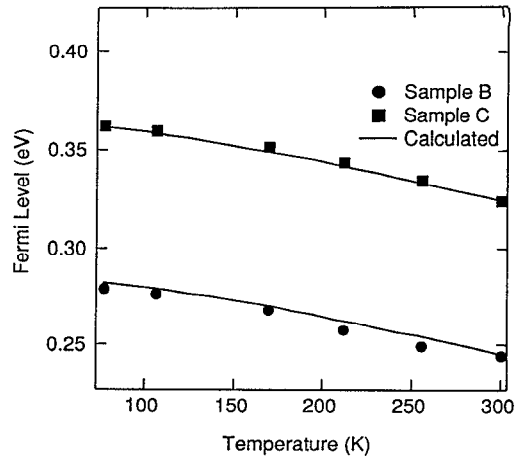


FIG. 3. Fermi level as a function of temperature for samples B and C. Solid lines show the temperature dependence of the band gap.

close to the conduction-band edge. Therefore the lineshape is not as sensitive to the exact position of the Fermi level. As a consequence the error on the fitted values is significantly larger (about 5 meV). Our measurements indicate that the “intrinsic” sample A is also degenerate. This can be explained by the significant background doping level in the hetero-epitaxial layer. For the measurement at 300 K there is an additional contribution of thermally excited carriers ( $n_i = 6 \times 10^{16}$  at 300 K for  $x = 0.7$ ).<sup>21</sup>

## V. DETERMINATION OF ELECTRON CONCENTRATION AND COMPARISON WITH ELECTRICAL MEASUREMENTS

From the Fermi level one can calculate the carrier concentration with Eq. (11). Figure 4 shows the calculated carrier concentration as a function of the Fermi level at 77 and 300 K. At high energies ( $> 100$  meV above the band gap), the shape of the curves is almost identical but there is a shift,

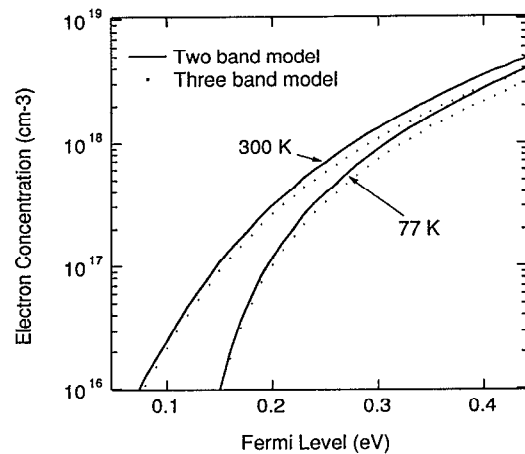


FIG. 4. Calculated electron concentration vs Fermi level at 77 and 300 K with the two band model (solid line) and the three band model (dots).

caused by the temperature dependence of the band gap. The fitting procedure to determine the Fermi level from absorption measurements is very insensitive to the two-band approximation. This can be explained by the fact that the absorption spectrum consists of the product of a slowly varying envelope, determined by the density of states, multiplied by a distribution function that varies rapidly around the Fermi level. The two-band approximation results in a slightly different envelope function, resulting in a considerable error on the fitted value of  $K$ , but only causing a minor error on the value of the Fermi level. In contrast, the carrier concentration as determined from the fitted Fermi level, is much more sensitive to the precise value of the density of states. For comparison we have worked out Eq. (11) numerically with the three band model<sup>12-14</sup> assuming  $\Delta = 0.75$  eV (linear interpolation between  $\Delta_{\text{InAs}} = 0.4$  and  $\Delta_{\text{InSb}} = 0.9$ ). The results are added to Fig. 4 (dots). The agreement is quite good but at large energies there is an increasing deviation.

For the undoped sample (A) we find an  $n$ -type background doping level of  $4.4 \times 10^{16} \text{ cm}^{-3}$  at 77 K. This high value is due to the large mismatch between the epilayer and the substrate (12.5%). At 300 K the measured electron concentration is  $9.7 \times 10^{16} \text{ cm}^{-3}$ . The increase can be explained by the thermal excitation of electrons above the narrow band gap.

The calculated carrier concentrations are listed in Table III together with the results of SIMS, Hall, and stripping Hall measurements. The SIMS measurements give the actual number of Si atoms in the epilayer and were calibrated using implanted reference samples. The electrical characterization of  $\text{InAs}_{1-x}\text{Sb}_x$  using Hall measurements is not straightforward. No lattice matched substrates are available for  $\text{InAs}_{1-x}\text{Sb}_x$  so that this type of material always has to be grown mismatched. The most suitable substrate from this point of view is InSb (2.0% mismatch). Even for those substrates, the mismatch gives rise to a significant dislocation density at the heterointerface so that electrical measurements on thin epilayers are always complicated by the presence of electrically active defects in the interface region. In this study we used GaAs (12.5% mismatch) and Si (17% mismatch) as substrates. These substrates are very attractive for the monolithic integration of infrared detectors with

TABLE III. Carrier concentration from optical measurements ( $N_{\text{opt}}$ ) using the two-band and three-band approximations and from SIMS, Hall, and stripping Hall measurements.

Sample	A	B	C
$N_{\text{opt}}-300 \text{ K}$ ( $10^{17} \text{ cm}^{-3}$ )			
Two band	1.1	6.5	17
Three band	0.97	5.4	14
$N_{\text{opt}}-77 \text{ K}$ ( $10^{17} \text{ cm}^{-3}$ )			
Two band	0.50	6.4	19
Three band	0.44	5.3	15
$N_{\text{SIMS}}$ ( $10^{17} \text{ cm}^{-3}$ )	...	3.7	37
$N_{\text{Hall}}-300 \text{ K}$ ( $10^{17} \text{ cm}^{-3}$ )	5	15	70
$N_{\text{Stripping Hall}}-300 \text{ K}$ ( $10^{17} \text{ cm}^{-3}$ )	...	4	30

electronic devices. Detailed information relative to the quality of the epitaxial layers grown on such highly mismatched substrates is given in Ref. 4. Due to the large mismatch, the interpretation of Hall measurements is particularly difficult. Standard Hall measurements systematically give a carrier concentration that is much larger than the expected value. The optical measurements that are analyzed in this paper are not strongly influenced by the crystal defects and the major contribution comes from the bulk-like material so that the optically determined carrier concentration is expected to be a good estimate. The accuracy of the Hall measurements can be significantly improved by using the stripping Hall technique, the results of which are also added to Table III.<sup>4</sup> The results of all different techniques are summarized in Fig. 5 which shows the carrier concentration as a function of the inverse Si cell temperature. For comparison we added experimental data of Si-doped GaAs samples. We also added the results of Si-doped  $\text{InAs}_{1-x}\text{Sb}_x$  layers with slightly different compositions that were grown in a different run. A good agreement between the reference measurements and the SIMS, stripping Hall and optical measurements was found for Si temperatures between 950 and 1050 °C. At higher Si-cell temperatures, the active Si doping level decreased, demonstrating an autocompensation effect. In Ref. 3, Parker *et al.* describe similar observations for the Si-doping of InSb. For low Si-cell temperatures, the background doping level and the intrinsic carrier concentration become important, resulting in a higher electron concentration in  $\text{InAs}_{1-x}\text{Sb}_x$  compared with GaAs. This is clearly illustrated by the measurements on the "undoped" sample A which were added on the right of Fig. 5.

## VI. HEAVY DOPING EFFECTS IN $n$ -TYPE $\text{InAs}_{0.3}\text{Sb}_{0.7}$

At high doping levels the bandstructure may significantly deviate from the intrinsic band structure. Since detailed studies of heavy doping effects in InAs or in InSb are

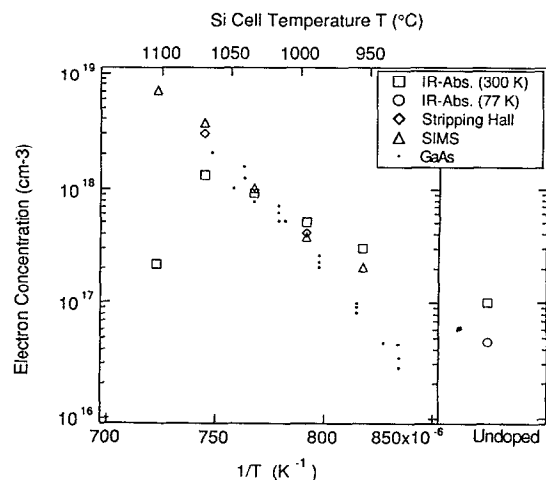


FIG. 5. Electron concentration vs inverse Si temperature for  $\text{InAs}_{1-x}\text{Sb}_x$  determined optically (squares: 300 K and circles: 77 K), from stripping Hall measurements (diamonds), and SIMS measurements (triangles). The dots are from Hall measurements on reference GaAs samples.

not available in literature, we will give a rough estimation of band-gap narrowing (BGN). We will assume that the total shrinkage  $\Delta E_g$  of the band gap can be thought as a sum of three contributions. The first is the “correlation” contribution arising from the electrostatic screening of electrons among themselves. The second contribution is the purely quantummechanical exchange effect, while the last contribution is a distortion of the density of states causing band-tails due to the random distribution of impurities in the intrinsic lattice.

An estimate for BGN due to correlation is calculated from

$$\Delta E_{g\text{cor}} = \frac{q^2}{4\pi\epsilon} \kappa, \quad (13)$$

where  $\kappa$  denotes the inverse screening length. It is found<sup>23</sup> that for practical doping levels, this effect dominates in GaAs. However, due to the large effective Bohr radius, the inverse screening length in InAs and InSb is relatively small compared to GaAs. For InAs<sub>0.3</sub>Sb<sub>0.7</sub> we took an effective mass of  $0.01m_0$ <sup>21</sup> and we linearly interpolated the permittivity between InAs and InSb, yielding  $16.7\epsilon_0$ . For doping levels of  $5 \times 10^{17}$  and  $3 \times 10^{18} \text{ cm}^{-3}$  we found that  $\Delta E_{g\text{cor}}$  varied from 5.5 to 7.5 meV in InAs<sub>0.3</sub>Sb<sub>0.7</sub> and from 19 to 26 meV in GaAs. The influence of the exchange effect,  $\Delta E_{g\text{ex}}$ , is estimated from Inkson’s model<sup>24</sup>

$$\Delta E_{g\text{ex}} = \frac{q^2}{2\pi^2\epsilon} [k_F - \kappa \arctan(k_F/\kappa)]. \quad (14)$$

Due to the highly nonparabolic bandstructure, InAs<sub>0.3</sub>Sb<sub>0.7</sub> exhibits a larger exchange contribution than GaAs:  $\Delta E_{g\text{ex}}$  ranges from 9 to 21 meV in InAs<sub>0.3</sub>Sb<sub>0.7</sub>, while from 5 to 13 meV in GaAs for  $n$  varying from  $5 \times 10^{17}$  to  $3 \times 10^{18} \text{ cm}^{-3}$ . The Fermi level shift arising from a tailed density of state (DOS) function, is approximated by

$$\Delta E_{g\text{tail}} = \frac{1}{\sqrt{\pi} \rho_{\text{int}}(E_F)} \int_0^\infty N_{\text{int}}(\eta t) \exp(-t^2) dt, \quad (15)$$

where  $\rho_{\text{int}}(E)$  and  $N_{\text{int}}(E)$  are the intrinsic DOS, respectively integrated DOS, and  $\eta$  denotes the mean square potential energy. Although this formula can be obtained as a generalization of the semiclassical bandtail theory<sup>25</sup>, its derivation can be found in Ref. 26. This semiclassical approach describes very well the bandtails of majority carriers. Assuming a parabolic intrinsic DOS,  $\rho_{\text{int}}(E)$ ,  $\Delta E_{g\text{tail}}$  in GaAs varies from 3 to 6 meV for  $n$  going from  $5 \times 10^{17}$  to  $3 \times 10^{18} \text{ cm}^{-3}$ . For the narrow-band material InAs<sub>0.7</sub>Sb<sub>0.3</sub>, a more appropriate intrinsic DOS, derived from Eq. (1), was used. The resulting  $\Delta E_{g\text{tail}}$  is less than 1 meV for  $3 \times 10^{18} \text{ cm}^{-3}$  and, hence, bandtailing may be neglected.

For sample C, the carrier concentration as determined from SIMS is more than the double of the value that was derived from the optical measurement. We believe that this discrepancy is essentially due to the amphoteric behavior of Si at high doping levels. However it could as well be explained by a lowering of the Fermi level by 60 meV. The estimation for BGN suggests a lowering of the Fermi level of about 30 meV due to heavy doping effects. Therefore we

conclude that both effects (compensation and band-gap narrowing) could be important. Figure 5 also shows a sample grown with the Si cell at 1110 °C. While the SIMS measurement clearly shows a large Si incorporation ( $\approx 10^{19} \text{ cm}^{-3}$ ), the optical measurements reveal a very low bandfilling. This large discrepancy is almost completely due to the compensation effect of Si.

## VII. CONCLUSIONS

We have studied the infrared absorption spectra of Si-doped InAs<sub>1-x</sub>Sb<sub>x</sub> samples grown on large band-gap GaAs and Si substrates. Using an analytical expression for the absorption coefficient that was derived from the Kane band model, we could accurately fit the experimental curves and determine the Fermi level. This value was used to calculate the electron concentration and the results were compared with doping levels obtained from SIMS and Hall measurements. We also evaluated the importance of heavy doping effects in InAs<sub>1-x</sub>Sb<sub>x</sub>.

## ACKNOWLEDGMENTS

The authors would like to acknowledge W. Van de Graaf for excellent MBE support. We kindly acknowledge the assistance of L. Geenen (SIMS), P. Roussel (SEM), A. Demesmaeker, and H. Bender (WDS). W. Dobbelaere thanks the “Instituut tot aanmoediging van het Wetenschappelijk Onderzoek in Nijverheid en Landbouw (IWONL)” for financial support.

<sup>1</sup>S. R. Kurtz, L. R. Dawson, Thomas E. Zipperian, and R. D. Whaley, IEEE Electron Device Lett. **11**, 54 (1990).

<sup>2</sup>S. R. Kurtz, L. R. Dawson, R. M. Biefeld, I. J. Fritz, and Thomas E. Zipperian, IEEE Electron Device Lett. **10**, 150 (1989).

<sup>3</sup>S. D. Parker, R. L. Williams, R. Droopad, R. A. Stradling, K. W. J. Barnham, S. N. Holmes, J. Laverty, C. C. Phillips, E. Skuras, R. Thomas, X. Zhang, A. Staton-Bevan, and D. W. Pashley, Semicond. Sci. Technol. **4**, 663 (1989).

<sup>4</sup>J. De Boeck, W. Dobbelaere, M. Van Hove, J. Vanhellefont, W. De Raedt, W. Vandervorst, R. Mertens, and G. Borghs, Mater. Res. Soc. Symp. Proc. **198**, 147 (1990), Vol. 198, p. 147.

<sup>5</sup>J. -I. Chyi, S. Kalem, N. S. Kumar, C. W. Litton, and H. Morcoç, Appl. Phys. Lett. **53**, 1092 (1988).

<sup>6</sup>J. -I. Chyi, D. Biswas, S. V. Iyer, N. S. Kumar, H. Morkoç, R. Bean, K. Zanio, H. -Y. Lee, and H. Chen, Appl. Phys. Lett. **54**, 1016 (1989).

<sup>7</sup>W. Dobbelaere, J. De Boeck, and G. Borghs, Appl. Phys. Lett. **55**, 1856 (1989).

<sup>8</sup>W. Dobbelaere, J. De Boeck, M. Van Hove, K. Deneffe, W. De Raedt, R. Mertens, and G. Borghs, IEDM Tech. Digest, 717 (1989).

<sup>9</sup>W. Dobbelaere, J. De Boeck, M. Van Hove, K. Deneffe, W. De Raedt, R. Mertens, and G. Borghs, Electron. Lett. **26**, 259 (1990).

<sup>10</sup>E. Burstein, Phys. Rev. **93**, 632 (1954).

<sup>11</sup>T. Moss, Proc. Phys. Soc. B **67**, 775 (1954).

<sup>12</sup>E. O. Kane, J. Phys. Chem. Sol. **1**, 249 (1957).

<sup>13</sup>E. O. Kane, *Physics of III-V compounds*, Edited by R. K. Willardson and A. C. Beer (Academic, New York, 1966), Vol. 1.

<sup>14</sup>E. O. Kane, *Narrow Bandgap Semiconductors, Physics and Applications*, edited by W. Zawadzki, Lect. Notes (Springer Verlag, Berlin, 1980), Vol. 133.

<sup>15</sup>Gerald Bastard, *Wave Mechanics Applied to Semiconductors Heterostructures* (Les Éditions de Physique, Les Ulis Cedex, 1988).

<sup>16</sup>H. C. Casey and Frank Stern, J. Appl. Phys. **47**, 631 (1976).

<sup>17</sup>J. S. Blakemore, *Semiconductor Statistics* (Dover, New York, 1987).

<sup>18</sup>W. Kaiser and H. Y. Fan, Phys. Rev. **98**, 966 (1955).

<sup>19</sup>E. J. Johnson, *Semiconductors and Semimetals*, edited by R. K. Willardson and A. C. Beer (Academic, New York, 1967), Vol. 3, p. 176.

- <sup>20</sup>See e.g. O. S. Heavens, *Physics of Thin Films*, edited by G. Hass and R. E. Thun (Academic, New York, 1964); J. A. Stratton, *Electromagnetic Theory* (McGraw-Hill, New York, 1941); H. Y. Fan, Rept. Prog. Phys. **19**, 121 (1956).
- <sup>21</sup>A. Rogalski, Prog. Quant. Electr. **13**, 191 (1989).
- <sup>22</sup>G. W. Gobeli and H. Y. Fan, Phys. Rev. **119**, 613 (1960).
- <sup>23</sup>P. Van Mieghem, R. P. Mertens, G. Borghs, and R. J. Van Overstraeten, Phys. Rev. B **41**, 5952 (1990).
- <sup>24</sup>J. C. Inkson, J. Phys. C **9**, 1177 (1976). See also R. A. Abram, G. J. Rees, and B. L. Wilson, Adv. in Phys. **27**, 799 (1978). A more detailed discussion can be found in K. F. Berggren and B. E. Sernelius, Phys. Rev. B **24**, 1971 (1981).
- <sup>25</sup>See, e.g., A. L. Efros, Sov. Phys. -JETP **32**, 479 (1971); A. L. Efros, Sov. Phys.-Usp. **16**, 789 (1974); E. O. Kane, Phys. Rev. **131**, 79 (1963).
- <sup>26</sup>P. Van Mieghem, *Theory of Bandtails in Heavily Doped Semiconductors*, Imec, Internal report, 1990.